Isomer-Selected Vibrational Spectra of Solvated 2-Fluoropyridine Clusters with Water and 2,2,2-Trifluoroethanol Mixture: Effect of Cluster Formation on Conformation and Solvation Structure

Yuji YAMADA[1)], Yusuke NOBORU[1)], Takuma SAKAGUCHI[1)], and Yoshinori NIBU[1)]

(Received May 31, 2012)

Abstract

The cluster size-selected electronic spectra and the vibrational spectra in the CH and OH stretching vibrational region of the 2-fluoropyridine-(2,2,2-trifluoroethanol: TFE)$_m$(H_2O)$_n$ (m = 1, 2, n = 0-2) clusters in a supersonic jet has been investigated with a fluorescence-detected infrared (FDIR) spectroscopy and quantum chemical calculations. Several bands are observed in the lower frequency region of the electronic spectrum than the S_1 - S_0 origin transition of bare 2FP. From the support of the density functional theory calculation as well as analyzing the FDIR spectra obtained by fixing the probe frequencies to these bands, they are assigned to the origin bands of 2-fluoropyridine-TFE$_m$W$_n$ (m = 1, 2, n = 0-2). It is common to the observed clusters that they form chain structures containing the weak interaction of the pyridyl CH with the fluorine or oxygen atom in the terminal TFE. The detectable conformation of TFE in all the clusters is gauche only even in the case of the existence of the strong base such as 2-fluoropyridine. As for the conformation of TFE, the calculated result of the potential energy curve against the torsional dihedral angle shows that *trans*-TFE is much less favorable than *gauche*-TFE, especially, in the case of hydrogen bond (H-bond) donor, there is no local minimum around *trans*-conformation. Comparing the less preference of bare or H-bonded *t*-TFE to the case of ethanol, we suggest that this difference is attributed to the decreasing hyperconjugation among several dominant orbitals, and that the dominant factor of the conformational preference is hyperconjugation between the OH group and CC or CH bonds rather than the intramolecular OH···F H-bond. The preference of the terminal TFE in the mixed clusters with TFE and water solvents is observed, which is ascribed to the stronger cooperative effect of TFE than water. With respect to the solvation order, we consider it to be important to elucidate the preference of the terminal TFE in the H-bond network. That is because these results in the gas phase may help to understand the microscopic H-bond network structure around peptides or proteins in TFE-W mixed solution.

[1)] Department of Chemistry, Faculty of Science, Fukuoka University, 8-19-1 Nanakuma, Jonan-ku, Fukuoka, 814-0180, Japan

INTRODUCTION

2,2,2-Trifluoroethanol (TFE) has been widely known as a co-solvent employed in a number of studies on structural function which is of great importance in protein and peptide folding since the TFE added in solution likely promotes the formation of secondary structure of protein or stabilizes the native formation of secondary structure of peptides modeled in an aqueous solution[1-3]. A large number of studies using NMR spectroscopy and molecular simulation have suggested that, although under the usual conditions many peptides do not form native-like secondary structure in aqueous solution, the appropriate concentration of TFE increases the stability of various secondary structure-forming peptides[4-9]. For example, Howard and coworkers[6] revealed that low TFE concentration stabilizes tertiary structure of a model protein such as Hen egg white lysozyme, while higher one denatures it. In order to understand the stabilization or denaturation mechanism in the different TFE concentration, many investigations on the physical and chemical properties of TFE have highlighted the microscopic interaction between TFE and proteins[10-13]. Buck et al.[11] and Yang et al.[12] have demonstrated that TFE interacts with carbonyl oxygen atoms in peptide group and with hydrophobic part within intact proteins. On the other hand, Roccatano and coworkers[13] have recently suggested that the weak hydrophobic interaction between TFE and non-polar side chain of peptide models is not negligible. Thus, since the circumstance is different dependently on truncated protein models, it is difficult to establish the common description about the solvation structure and its effect upon the stability of secondary structure.

The studies on isolated clusters in supersonic jets[14] are known as one of the most available indicators to elucidate the microscopic solvation mechanism in such complicated systems. A lot of hydrogen-bonded (H-bonded) aromatic molecular clusters with water, methanol, ammonia, etc., have been investigated for a long time with respect to not only solvation structure[15-23] but also various relaxation dynamics in the electronically ground, i.e. S_0[23,24], and the first excited states, i.e. S_1[25-32]. However, the study on the H-bonded clusters containing TFE as a solvent is limited. In the early 1990's, Marco et al.[33,34] have reported H-bonded complexes of TFE with strong bases, such as ammonia, diethyl ether and pyridine in vapor phase through FTIR study. Recently, Suhm's group has carried out slit-jet FTIR experiments of TFE_n clusters[35,36]. Venkatesan and coworkers have researched the 1,2,4,5-tetrafluorobenzene (TFB) clusters with TFE and methanol in order to study aromatic CH···O interaction as a solvation model possessing a relatively weak interaction. As a result of their experiment, it has been found that the relatively weak CH···O interaction is present for the solvated clusters with methanol solvents, while absent for TFE one[37]. Thus, we insufficiently have obvious information to elucidate the H-bond network structure and its function to stabilize or denature peptides and proteins. In addition to the H-bond interactions, with regard to the mixed cluster as a model of the different concentration of aqueous TFE solution, an important factor is the "solvation order", namely, which solvent forms the first solvation shell and which is at the end of a solvent network. It is intriguing to focus on the H-bond strength and cooperative effect[38] in the

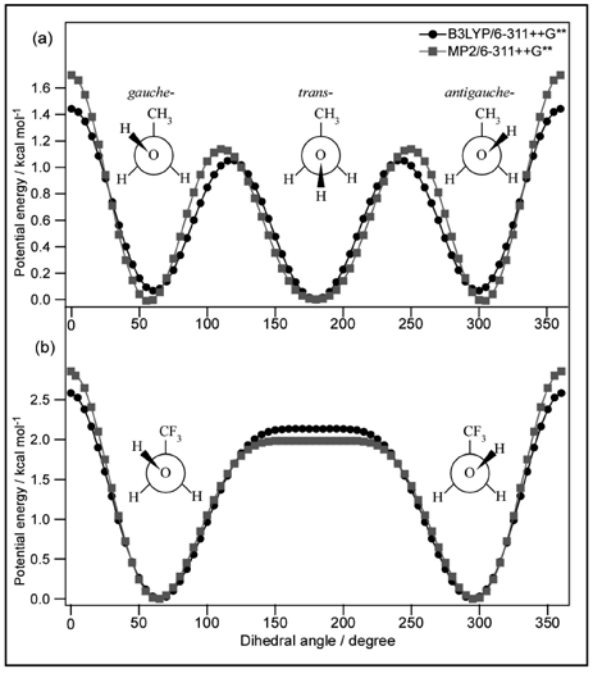

Fig. 1. Calculated potential energy curves of (a) ethanol and (b) TFE as a function of the HOCC dihedral angle. The calculations at the B3LYP and MP2 levels with the 6-311++G** basis set were performed by optimizing the geometry with the fixed dihedral angle.

mixed water and TFE clusters.

Another topic which should be introduced here is about the conformation of TFE. As broadly known in ethanol, three conformations are expected for the relative orientation between OH and CF_3 group in TFE; one is trans (*t*) conformation where the dihedral angle of HOCC is around 180 degree. The second and third belong to two energetically equivalent enantiomers having the "coiled" structure, where dihedral angles of HOCC are about +60 and −60 degree. In this article, they are denoted as gauche (*g*) and antigauche (*a*), respectively. In ethanol having a similar structure to TFE, almost equivalently stable three conformers exist in the gas[39,40] and the condensed phases[41] as well as in the matrix isolation[42]. Figure 1(a) shows the calculated potential energy curves against the dihedral angle in bare ethanol with two calculation methods. The two calculation levels exhibit similar results that the energies of three conformers are close. However, a similar calculation for bare TFE illustrates the different feature as seen in Fig. 1(b). The calculation reveals that *t*-conformer is remarkably unstable because the local minimum around *t*-conformation is too shallow to be present stably. Experimentally, vapor phase IR[33,43-46], Raman[43] and microwave[47], and slit-jet FTIR[35,36] spectroscopic results have demonstrated that the *g*-TFE conformer is dominant for TFE monomer. Furthermore, Scharge and co-workers[35] indicated that *t*-conformation of TFE may start to become important for a larger cluster than trimer, which supports the experimental observation of *t*-TFE in the condensed phase as reported by Bakó and coworkers[48]. They have proposed that the conformational preference of *g*-TFE originates from the intramolecular H-bond interaction between the electro-negative fluorine atom and the OH group[33,34,46-49]. Moreover, as mentioned above, in the vapor phase FTIR studies, Marco and coworkers[33,34] pointed out that the formation of intermolecular H-bonds with the strong bases breaks the intramolecular OH···F bond. However, their spectral resolution is too low to determine its conformation discriminately. On the other hand, the recent theoretical research of Senent et al.[50] has indicated that the repulsion forces between oxygen and fluorine atoms predominantly determines the conformational stability of TFE clusters. However, since the energy difference and barrier between *g*- and *t*-TFE are greatly dependent on the calculation level and the experimental analysis by some groups, the main factor determining the conformational preference has been in no consensus among various researchers.

In this work, we concentrate on the solvation structure of the mixed TFE and water (W), and the presence of *t*-TFE in the H-bonded clusters with the strong base such as 2-fluoropyridine (2FP). By applying the Laser-induced fluorescence (LIF) and fluorescence-detected IR (FDIR) measurements to the H-bonded clusters in supersonic jets, we obtain isomer-selected vibrational spectra to determine the TFE conformation and solvation structure among the water-TFE mixed solvents. The assignment of the vibrational spectra is carried out by means of the density functional theory (DFT) calculations on the basis of the previous assignment of several H-bonded 2FP clusters reported by our group[51-53]. Furthermore, the stability of *t*- and *g*-conformers of TFE is compared with the ethanol case in order to elucidate the origin of conformational preference.

EXPERIMENTAL and THEORETICAL

A detailed description of the experimental setup was given in the previous papers[51-53]. Brief picture of our experimental setup is seen in Fig. 2.

Supersonic jet method

The jet-cooled 2FP-TFE-water mixed clusters were generated by a supersonic expansion of their

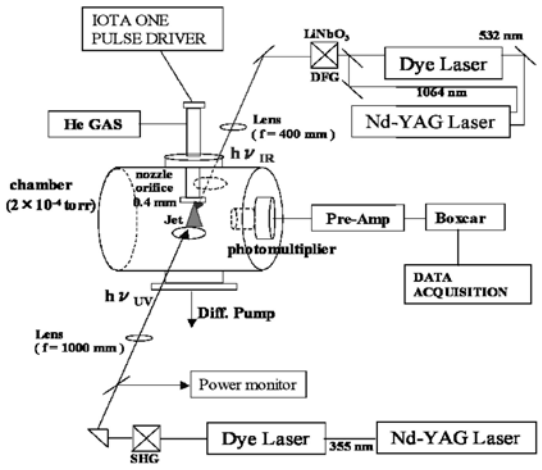

Fig. 2. Experimental setup for applying IR-UV spectroscopy to the molecular clusters in supersonic jets.

vapor seeded in He carrier gas (typically 3 atm) into vacuum through a pulsed nozzle (General valve, series 9) having a 1.0 mm aperture. A vacuum chamber was evacuated with diffusion pump (ULVAC, ULK-06) assisted by rotary pump (Alcatel, T2033SD), which typically keeps the pressure of 1.0 x 10^{-4} torr without the nozzle operation. A pulse duration of the nozzle was controlled with the pulse driver (IOTA ONE), typically with the duration of about 150 μs.

Tunable UV and IR laser setup

A tunable UV laser radiation was obtained with a frequency-doubled dye laser (Sirah, CSTR-G), which was pumped by a frequency tripled Nd:YAG laser (Spectra Physics, INDI-40). The UV laser radiation was introduced into the vacuum chamber and focused at the 10 mm downstream from the nozzle exit with a lens of 800 mm focal length. LIF spectra were detected with a photomultiplier tube (Hamamatsu Photonics, R-928). A tunable IR laser pulse for the OH/CH stretching vibrational region was generated with a differential frequency generation (DFG) in a $LiNbO_3$ crystal (Inrad, Autotracker III) with the fundamental light of a Nd:YAG laser (Spectra Physics, GCR-130) and the output of a dye laser (LAS, LDL-205) with LDS 759/821 dye, that is excited by the frequency doubled same Nd:YAG laser. The tunable IR radiation was introduced from the counter propagating direction against the UV laser. The time intervals among the nozzle driver, the IR laser and UV one were controlled with a digital delay generator (SRS, DG-535) and homemade pulse generator. IR spectra were recorded as a decrease of LIF intensity due to the vibrational transition induced by the tunable IR laser.

Theoretical

Our theoretical analysis for the geometry optimization and vibrational frequency of the relatively small 2FP-TFE$_m$-W$_n$ clusters ($m \leq 2$, $n \leq 2$) in the S_0 and S_1 states were carried out by the DFT calculation with Becke-three-parameter-LYP (B3LYP) functional and *ab initio* calculation with CI-Singles (CIS) level, respectively. The basis set of 6-311++G** was used in all the calculations. Scaling factor of 0.9561 was adopt in the vibrational frequency calculations at B3LYP level to reproduce the observed OH stretching frequency of *g*-TFE monomer, 3657 cm^{-1}[43]. Natural bond orbital (NBO) analysis with the B3LYP level and the second-order Møller-Plesset perturbation (MP2) theory was done by using the NBO program (NBO ver. 3.0). Since the natural population is sensitive to calculation levels, MP2 was added in this analysis. In evaluating the relative stabilization energies of the cluster isomers, we also corrected the basis set superposition error (BSSE) by a counterpoise method and carried out the zero-point vibrational energies correction (ZPC). In order to perform these calculations, we utilized Gaussian 03 program package[54]. The computation was carried out using the computer facilities at Research Institute for Information Technology, Kyushu University.

RESULT

Electronic spectrum of 2FP-TFE$_m$W$_n$

The 2FP clusters solvated by the mixed solvents with different composition and different conformers, such as gauche or trans, may offer the different electronic transition energies. Therefore, first of all, various clusters should be identified by observing the electronic transition originated from each cluster. Figure 3(a) shows the LIF spectra of bare 2FP and its hydrated clusters. As reported by Nibu and coworkers[51], the extremely strong band at 38019 cm^{-1} is assigned to the origin band of bare 2FP, while weaker bands at 38015 and 37945 cm^{-1} correspond to 2FP-W$_1$ and -W$_2$ clusters, respectively. The addition of TFE gives us the further appearance of some new bands, as seen in Fig. 3(b). The values in the figure

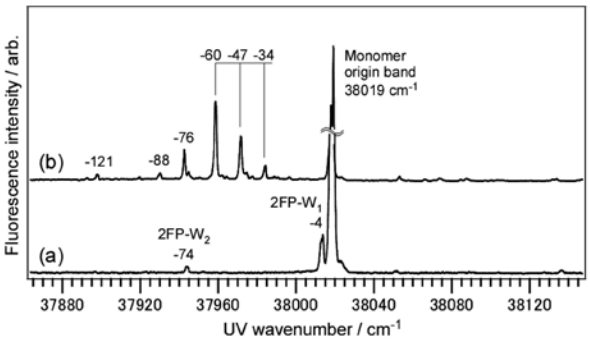

Fig. 3. LIF spectrum of bare 2FP and its hydrated clusters. The origin band of bare 2FP is observed at 38019 cm^{-1}. (b) LIF spectrum of 2FP-TFE$_m$W$_n$ clusters. The values in the figure indicate the frequency shifts from the origin band of bare 2FP.

indicate the shift from the origin band of bare 2FP, 38019 cm^{-1}. The vibrational progression having the same interval of 13 cm^{-1} is observed from the band at −60 cm^{-1}, and several very weak bands appear at −76, −88 and −121 cm^{-1}. In the suppression of the TFE vapor pressure by cooling the sample bottle of TFE, the sequential three bands with 13 cm^{-1} interval maintain sufficiently strong intensity despite the disappearance of the other bands. Besides, it is interesting that the bands originated from 2FP-W_n (n = 1, 2) clusters disappear. The disappearance of their signals implies not the lack of water molecules within the supersonic expansion, but the relatively decreasing abundance of the solvated 2FP clusters with water. Therefore, we should consider the existence of the mixed clusters with water and TFE solvents in the assignment of these observed bands.

Vibrational spectra of 2FP-TFE_mW_n

Figure 4 shows the FDIR spectrum of the OH stretching vibrational region obtained by scanning IR frequency with fixing the UV frequency to the −60 cm^{-1} band in the LIF spectrum. The FDIR spectra at the probe of −34 and −47 cm^{-1} are identical to that of −60 cm^{-1}, meaning that these three bands are originated from the same cluster. In the lower frequency region, the strong and broad band is

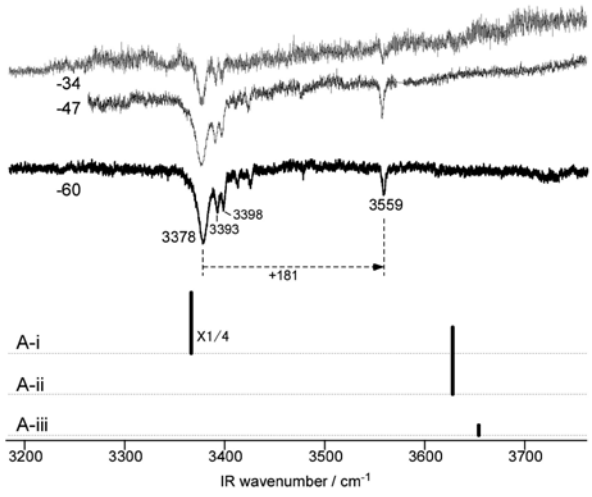

Fig. 4. FDIR spectra with the probe UV laser fixed to the −60, −47 and −34 cm^{-1} bands in the LIF spectrum. The lower inserts are the simulated spectra of various isomers for 2FP-TFE1 calculated at the B3LYP/6-311++G** level. Their geometries and vibrational frequencies are listed in Fig. 8(a) and Table 1, respectively.

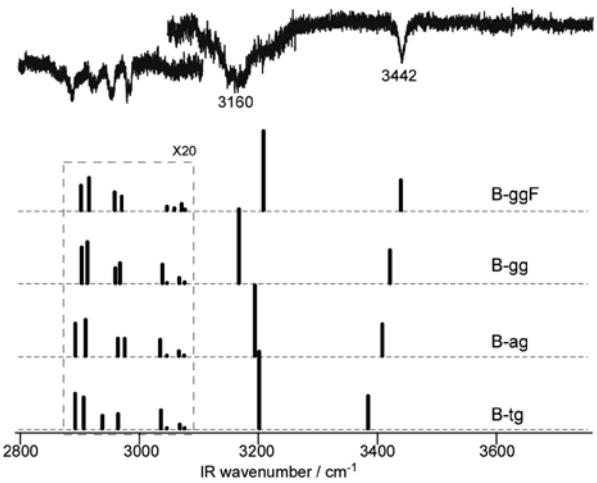

Fig. 5. FDIR spectrum in the region of the OH and CH stretching vibrations with the probe UV laser fixed to the −76 cm^{-1} band in the LIF spectrum. The lower inserts are the simulated spectra of various isomers for 2FP-TFE_2 listed in Fig. 8(b). The vibrational frequencies and the relative stabilization energies of them are summarized in Table 1. Because of small intensities of the CH stretching vibrations, the simulated IR spectra in the CH stretch region are expanded by twenty times in intensity.

observed at 3378 cm^{-1}, and the relatively weak bands are around it, i.e. 3393, 3398, 3413 and 3426 cm^{-1}. In the higher frequency region, on the other hand, a band appears at 3559 cm^{-1}, which is 181 cm^{-1} higher than the strong band at 3378 cm^{-1}, but no band is observed in the free OH stretching vibrational region around 3700 cm^{-1}. This result reveals that TFE forms an H-bond with 2FP and that this cluster includes no water as a solvent.

Figure 5 shows the FDIR spectrum probed at the frequency of −76 cm^{-1}. There are two bands in the OH stretching vibrational region; one is the considerably broad band observed around 3160 cm^{-1}, assigned to be derived from the very strongly H-bonded OH stretch. The other is at 3442 cm^{-1}, and there is no band in the region of the free OH stretching vibration. Since only two H-bonded OH bands are observed, it cannot be unambiguous to determine the structure of the cluster only from the OH band position, which will be mentioned in the discussion section. In order to get additional information about the solvation structure, the FDIR spectrum in the CH

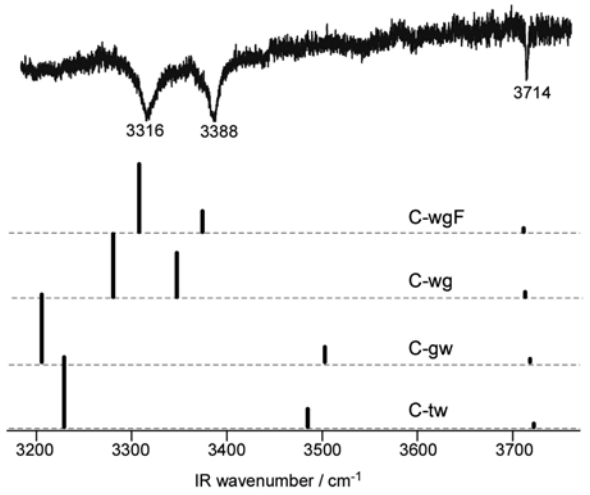

Fig. 6. FDIR spectrum with the probe UV laser fixed to the –88 cm^{-1} band in the LIF spectrum. The lower inserts are the simulated spectra of various isomers for 2FP-TFE_1W_1 listed in Fig. 8(c). The vibrational frequencies and the relative stabilization energies of them are summarized in Table 1.

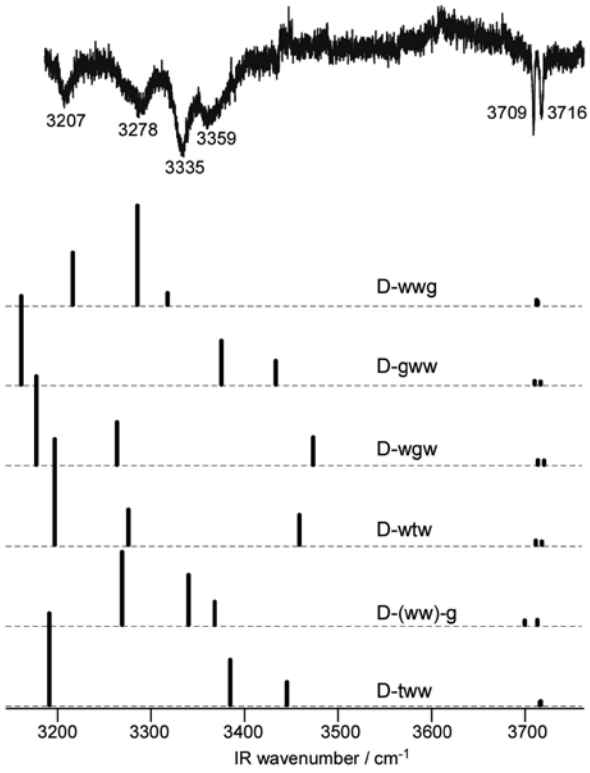

Fig. 7. FDIR spectrum at the probe frequency of the –121 cm^{-1} band in the LIF spectrum. The lower inserts are the simulated spectra of various isomers for 2FP-TFE_1W_2 listed in Fig. 8(d). The vibrational frequencies and the relative stabilization energies of them are summarized in Table 1.

stretch region was also measured. As seen in Fig. 5, there are several bands under 3000 cm^{-1} region. They are considered to be methylene CH stretching bands from the fact that the methylene CH ones of bare TFE are observed at 2974 and 2957 cm^{-1}[43], while the pyridyl CH ones are at the region between 3000-3150 cm^{-1}[55]. Because of the Fermi resonance of the CH stretching vibrations with the lower-frequency modes, for example, CH bending overtones[56], the bands are split into two peaks or broadened. But we can roughly classify them into four bands, that is 2886, 2921, 2954 and 2980 cm^{-1}. The result that the several methylene CH stretching bands are observed provides us a prediction that this cluster includes a few TFE molecules.

On the other hand, Figs. 6 and 7 show the FDIR spectra at the bands of –88 and –121 cm^{-1}, respectively. There are a few bands in the region of the free OH stretching vibration of H-bonded water, meaning that these bands are originated from the 2FP clusters composed of water and TFE solvents. Then, the several bands observed around 3300 cm^{-1} are assigned to the H-bonded OH stretching vibrations of water and/or TFE. The several IR spectra shown by bars below each experimentally observed spectrum in Figs. 4 to 7 are the calculated ones for the optimized structures which will be referred to in the next section. In the discussion section, the assignment of isomers will be examined by comparing these spectra to the experimental one.

Calculation of solvation structures

In order to clarify the cluster composition of water and TFE from the above-mentioned FDIR spectra, the DFT calculations have been performed. Figure 8 shows the optimized geometries of 2FP-TFE_mW_n. The calculated results of vibrational frequencies and relative stabilization energies for these isomers are also listed in Table 1. As obviously seen in Fig. 8(a), A-i isomer, which forms H-bond between the TFE donor and the 2FP acceptor, is the global minimum for 2FP-TFE_1. A-i is more stabilized than A-ii and A-iii by 3.7 and 3.9 kcal/mol, respectively. Here, it should be noted that the TFE moiety corresponds to *g*-conformer. On the other hand, *t*-TFE

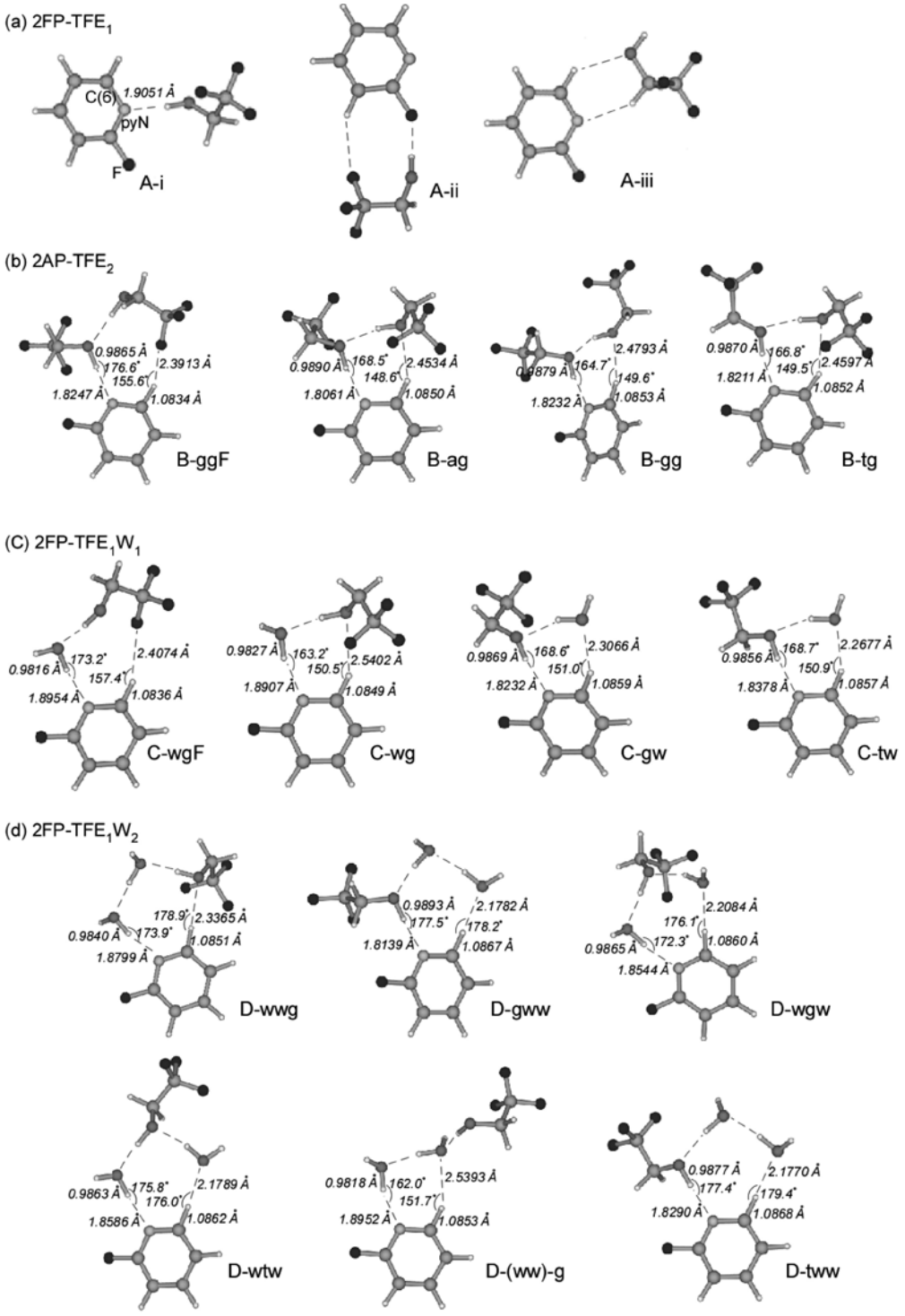

Fig. 8. Optimized geometries and relative stabilization energies in kcal/mol of (a) 2FP-TFE1, (b) $-TFE_2$, (c) $-TFE_1W_1$ and (d) $-TFE_1W_2$. The calculations were carried out at the B3LYP/6-311++G** level. The values in the figure indicate the bond length and angle among the atoms involved in H-bond.

is not obtained as a stable structure, implying that the considerably shallow or no minimum along the torsional coordinate around C-O bond in TFE. The cluster containing *a*-TFE exhibits the equivalent stabilization energy and has a symmetrical relationship to *g*-one with regard to reflection in the pyridine ring. This result as well as the experimental result that we cannot observe the splitting of the

electronic band within our experimental resolution indicates that this cluster includes no observable torsional tunneling. It may be because of the high barrier and the large mass along the torsional motion. Therefore, it is not necessary to take into account the cluster chirality. In addition, as indicated by the much shorter intermolecular length involved in this H-bond (1.9051 Å), A-i is considerably stabilized by the strong H-bond between the TFE OH group and the nitrogen atom in 2FP (hereafter denoted as pyN). Thus, in considering the stability of the clusters with a large number of TFE and water solvents, we will focus on the isomers forming the dominant H-bond of TFE OH···pyN.

Figure 8(b) shows the optimized structures for 2FP-TFE_2. The most stable four isomers form the chain structure where the cluster stability is mainly attributed to the two H-bonds between TFE OH··· pyN and between two TFE molecules. Here, two interesting findings are highlighted from these

Table 1. Calculated frequencies[a] in cm^{-1} and relative stabilization energies (E_{bind}) of isomers at the B3LYP level with the 6-311++G** basis set.

			2FP-TFE_1			
Isomer	A-i	A-ii	A-iii			
OH_{TFE}	3366	3628	3654			
E_{rel} (kcal/mol)	+0.0	+3.71	+3.90			
			2FP-TFE_2			
Isomer	B-ggF	B-ag	B-gg	B-tg		
OH_{TFE}	3209	3167	3194	3201		
OH_{TFE}	3440	3421	3408	3385		
E_{rel} (kcal/mol)	+0.0	+0.55	+0.75	+1.00		
			2FP-TFE_1W_1			
Isomer	C-wgF	C-wg	C-gw	C-tw		
OH_{TFE}	3374	3347	3206	3229		
$OH_{w\ (H\text{-}bond)}$	3308	3281	3503	3485		
$OH_{w\ (free)}$	3711	3713	3718	3722		
E_{rel} (kcal/mol)	+0.0	+0.26	+0.71	+1.53		
			2FP-TFE_1W_2			
Isomer	D-wwg	D-gww	D-wgw	D-wtw	D-(ww)-g	D-tww
OH_{TFE}	3318	3181	3264	3276	3368	3191
$OH_{w\ (H\text{-}bond)}$	3216	3375	3177	3197	3269	3385
$OH_{w\ (H\text{-}bond)}$	3285	3433	3473	3459	3340	3445
$OH_{w\ (free)}$	3712	3710	3714	3711	3700	3716
$OH_{w\ (free)}$	3713	3717	3720	3718	3711	3717
E_{rel} (kcal/mol)	+0.0	+0.78	+1.24	+1.53	+1.60	+1.99

[a] Scaling factor of 0.9561.

Table 2. Calculated frequencies in cm^{-1} and approximate description of intermolecular and the lowest intramolecular vibrations of isomer A-i in S_0 and S_1 states at the B3LYP and CIS levels with the 6-311++G** basis set, respectively.

				S_0			
Description[a]	τ	ρ_1	β_1	β_2	ρ_2	σ	τ_{CC}
Frequency[b]	8.0	18.3	19.9	49.9	61.0	99.6	184.6
				S_1			
Description[a]	τ	ρ_1	β_1	β_2	ρ_2	σ	τ_{CC}
Frequency[b]	17.9	22.5	40.1	49.1	55.0	93.3	161.8

[a] See ref. 19 for the nomenclature of intermolecular vibrations.

[b] Without scaling.

calculations. One is that *t*-TFE acting only as an H-bond donor is unlikely. We cannot obtain the local minimum corresponding to B-gt where *t*-TFE forms the outer solvation shell in the chain structure, which will be discussed in detail below. The other is the existence of the weak interaction between C-H at the sixth-position of pyridine ring (denoted as C(6)-H) and O/F atom in TFE. For example, as seen in the figure for B-ggF, the sufficiently short length between C(6)-H and F atom of TFE, 2.3913 Å, indicates that it is stabilized not only by the dominant H-bond chain but also by the additional weak H-bond between C(6)-H and F atom. This additional interaction may let us regard this chain structure as a cyclic structure in a sense. Interestingly, B-ggF possesses the additional interaction between C(6)-H···F atom, while the other isomers show that between C(6)-H···O atom. Although the C(6)-H bond length is elongated from 1.0819 Å in 2FP monomer in all the cases, the strength of the perturbations is different among the clusters. The C(6)-H bond length is 1.0834 Å for B-ggF, meaning that it is not so largely perturbed, while the greatly elongated ones of 1.0850 and 1.0852 Å for B-ag and B-tg, respectively, imply the stronger interaction of C(6)-H···O than C(6)-H···F. However, the fact that the angles of C(6)-H···O atom and of O-H···pyN for B-tg isomer are about 149° and about 167°, respectively, indicates that the whole H-bond network is distorted and unfavorable rather than the B-ggF case. Thus, in 2FP-TFE_2 case, the C(6)-H···F interaction is appropriate as a whole. One should note that several initial geometries which contain *a*-/*t*-TFE and a terminal *g*-TFE with the additional C(6)-H···F interaction relax toward B-ag/B-tg not B-agF/B-tgF during optimizations.

As for 2FP-TFE_1W_n, in addition to the conformation of TFE itself, the solvation order is an important factor. 2FP-TFE_1W_1 has two possibilities that either TFE or water molecule constructs the strong H-bond with pyN. From the viewpoint of 2FP solute, it is regarded as the first solvation shell, and the other molecule forms the H-bond with the first shell, corresponding to the second solvation shell. As seen in Fig. 8(c), C-wg, the chain structure of pyN-W-TFE, is the global minimum. Similarly to the case of B-ggF, C-wgF forms the appropriate configuration for the additional C(6)-H···F interaction. The second and third stable isomers of C-wg and C-gw have the inverse solvation order. Both isomers seem to form the additional H-bonds of C(6)-H···O, but the whole H-bond network is distorted and unfavorable rather than the C-wgF case. As for conformation, TFE is gauche in these cases. On the other hand, *t*-conformer provides the higher relative energy, for example, C-tw is 0.82 kcal/mol higher than C-gw despite the same solvation order. Furthermore, the terminal *t*-TFE is not obtained as a local minimum. As stated above, the TFE molecule, which acts as an H-bond donor on the second solvation shell, is unlikely to be *t*-conformation.

Finally, Fig. 8(d) shows the optimized geometries for 2FP-TFE_1W_2. The relatively stable isomers adopt the chain structure with the additional C(6)-H···O interaction, corresponding to the cyclic structure. In contrast to C-gw, the cyclic structure is not distorted due to the addition of a water molecule, resulting in the relatively strong H-bond network. As for D-wwg, D-wgw and D-gww, only the position of the *g*-TFE in the H-bond network is different. The most stable isomer of D-wwg is about 1 kcal/mol lower than the other two isomers. As the other size clusters, the isomers containing *t*-TFE is relatively unstable and especially D-wwt, i.e. 2FP-W-W-(*t*-TFE), is not obtained.

Discussion

Assignment of the clusters

Firstly, we determine the cluster composition, the solvation structures and the TFE conformation by comparing the observed IR spectra with the calculated results. As seen in Fig. 4, the strong band at 3378 cm^{-1} agrees well with the calculated OH stretching vibration (ν_{OH}) of A-i of 2FP-TFE_1, although several weak bands are observed. This agreement as well as the fact that the sequential three bands of −60, −47 and −34 cm^{-1} in LIF spectrum maintain sufficiently strong even in the condition of the suppressed-TFE vapor pressure suggests that these bands are assigned to 2FP-TFE_1. The other weak bands are considered to be due to Fermi resonance between the OH stretching vibration and the overtone/combination bands of the intramolecular modes, or due to the anharmonic coupling to the low-frequency modes such as intermolecular vibrations, leading to the sufficiently intense combination bands of the OH stretch and low-frequency mode, namely a

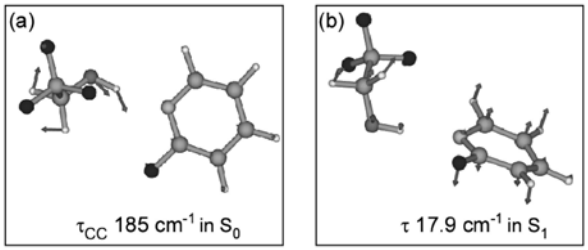

Fig. 9. Motional feature of (a) the torsional mode along the CC bond axis (τ_{CC}) and (b) the intermolecular torsional mode (τ), whose frequencies are calculated to be 185 and 17.9 cm^{-1}, respectively. Mode of τ is calculated at the geometry optimized with the CIS level under the restriction in the electronically firstly-excited state. See text and Table 2.

"Franck-Condon like" vibrational progression[57,58]. The H-bonded clusters forming the strong H-bond to pyN, for example, 2-aminopyridine[22] and 2FP[52], etc., represent the broadly and structured OH/NH stretching band or the additional overtone of OH/NH bending modes. The isolated band at 3559 cm^{-1} is 181 cm^{-1} higher than ν_{OH} at 3378 cm^{-1}, which is in good accordance with the vibrational frequency of the torsional mode along the CC bond axis (hereafter denoted as τ_{CC}) as listed in Table 2. The motional feature of the vibrational mode displayed in Fig. 9(a) demonstrates the large change in the length of OH⋯pyN. In conclusion, this band can be assigned to the combination band, $\nu_{OH} + \tau_{CC}$, and we consider that our above assignment can explain the experimental result displaying several bands in the IR spectrum. In addition to the IR spectrum, the fact that the lowest vibrational frequency (17.9 cm^{-1}) of A-i isomer in S_1 listed in Table 2 is close to the 13 cm^{-1} interval of the vibrational progression observed in the LIF spectrum may support our assignment. The motional feature of this mode is also seen in Fig. 9(b), where the pyridyl ring is calculated to be distorted remarkably, which is due to the weakened π conjugation upon $\pi\pi^*$ excitation.

Next, as shown in Fig. 5, the IR spectra in the OH and CH stretch regions for the −76 cm^{-1} band indicate that there are two H-bonded OH stretching bands, while no free OH stretching band is observed. This result easily provides us an idea that this cluster corresponds to 2FP-TFE_2. However, it is difficult to assign these bands definitely, since the simulated IR spectra for the four isomers are similar in the OH region and contain ambiguity about scaling factor and so on. On the other hand, the IR spectrum in the CH stretching region reveals that the CH_2 stretches of TFE are clearly observed and that the pyridyl CH ones do not possess enough band intensities to detect. The calculated intensities of C(6)-H stretches for B-wg, B-ag and B-tg are as large as the CH_2 ones of TFE because of the weak H-bond interaction. Thus, we assign the −76 cm^{-1} band in the LIF spectrum to B-ggF.

In Fig. 6, the calculated result of C-wgF for 2FP-TFE_1W_1 reproduces the IR spectrum best although that of C-wg also seems reasonable. Therefore, we conclude that the −88 cm^{-1} band in the LIF spectrum is ascribed to the C-wgF form, although the alternative assignment also might be feasible. The lower frequency H-bonded OH band is mainly assigned to the OH stretch of the water molecule (νOH_w) in the first solvation shell which forms the strong H-bond with pyN although these modes are partially mixed between the OH stretches of TFE (νOH_{TFE}) and νOH_w. However, this situation is slightly different in the case of analyzing the IR spectrum for 2FP-TFE_1W_2. As seen in Fig. 7, the IR spectrum is complicated, namely there are several broad bands in the H-bonded OH stretching region. The fact that there are two bands in the free OH stretching region indicates that the cluster consists of two water molecules at least. Besides, the simulated IR spectrum for D-wwg in Fig. 7 gives three H-bonded OH bands whose positions and intensities are in sufficiently good agreement with the experimental one, except for a band at 3207 cm^{-1}. It is worthwhile mentioning to the fact that the additional bands around 3200 cm^{-1} are observed in 2FP-W_2 cluster and assigned to the overtone of the OH bending modes of waters in the previous paper[52]. Therefore, we assign this additional band to the overtone of the OH bending mode, and it is concluded that the band at −122 cm^{-1} is originated from D-wwg of 2FP-TFE_1W_2. The calculated relative energies also support this assignment, although it might be not conclusive evidence due to the somewhat poor accuracy of the relative energy in DFT calculations with this level and basis sets. Three bands observed in the region of the H-bonded OH stretch, i.e. 3278, 3335 and 3359 cm^{-1} can be roughly classified into νOH_w directly combining to pyN,

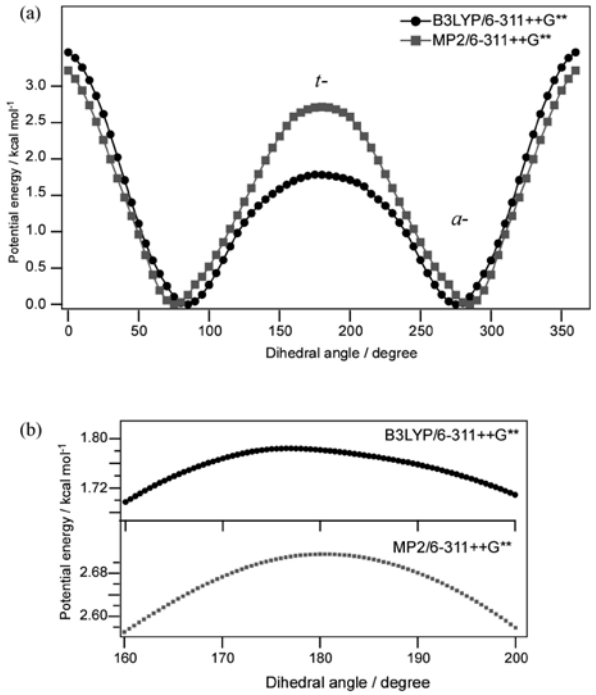

Fig. 10. Calculated potential energy curves of 2FP-TFE_1 as a function of the torsional dihedral angle of HOCC in TFE. The calculations at the B3LYP (black circle) and MP2 (gray square) levels with the 6-311++G** basis set were performed by optimizing the geometry with the fixed dihedral angle. (b) The expanded potential energy curves around 180-degree dihedral angle.

νOH_{TFE} of the terminal TFE and νOH_w in the second solvation shell, respectively.

Conformation of TFE

The above assignment provides two findings. One is favorable *g*-conformation, and the other is about the solvation order in the mixed TFE-W clusters; the terminal TFE is preferable, as C-wg and D-wwg. In this section, we argue about the former. The experimental results show that *t*-conformer is not observed in various cluster size. This is considered to be because of the large instability of *t*-conformer of the TFE moiety although TFE acts as various roles, such as H-bond donor and/or acceptor. Interestingly, our calculated results point out that, when TFE acts only as an H-bond donor, *t*-TFE has no local minimum, meanwhile *t*-TFE as an H-bond acceptor exhibits the sufficient stability. Figure 10 depicts the potential energy curves of 2FP-TFE_1 against the OH torsion. The calculated ones at both two levels unambiguously indicate that there is no minimum around 180-degree dihedral angle.

As for the conformation of TFE, a number of studies have interpreted that the favorable gauche conformer of bare TFE is due to the intramolecular H-bond with the fluorine atom[33,34,46-49]. However, our experimental and calculated results as well as the small difference of the OH stretching frequency of bare TFE and *g*-ethanol, 3657[43] and 3660 cm^{-1}[59], respectively, indicate that the intramolecular H-bond is too weak to stabilize *g*-TFE specially. Furthermore, the result that the stability of *t*-TFE is largely dependent on the H-bond roles lets us consider that the change in molecular orbitals may be mainly responsible for the stability change of *t*-TFE. Since the first suggestion by Wolfe[60], the gauche effect, that is the phenomenon of the preferable *g*-conformer in the ethanes 1,2-disubstituted by electronegative atoms, has been argued by many researchers[61-65]. They have shown that not steric effect but hyperconjugation, that is the donor-acceptor electron transfer or resonance structures, is primarily responsible for the gauche effect. Similarly, it is reasonable to take into account that hyperconjugation between the OH antibonding orbital (σ^*_{OH}) and C-X (X = H or CF_3) bonding orbitals (σ_{CH}/σ_{CC}) is dominant factor in the case of *g*-/*t*-TFE. This is depicted in the left side of Fig. 11(a). In addition, one should consider another two interactions between the nonbonding orbitals on the O atom corresponding to n_O-σ and n_O-π, and C-X anti-bonding orbitals (σ^*_{CH} or σ^*_{CC}), as displayed in the middle and right side of Fig. 11(a), respectively. Although the orbital energies and composition are slightly dependent on the conformation or the chemical substitution, we mainly discuss the above-mentioned three hyperconjugation only for simplicity. Figure 11(b) represents the schematic energy diagram about its difference between ethanol and TFE. The arrows indicate the donor-acceptor electron transfer in both conformers. If a CH_3 group is substituted by CF_3, the existence of the strongly electron-attractive fluorine atoms reduces the orbital energies of σ_{CC} and σ^*_{CC}. As a result, the interaction between σ^*_{OH} and σ_{CH} (at the trans position to the OH bond, t) for *g*-conformer remains, while $\sigma_{CC}(t) \rightarrow \sigma^*_{OH}$ for *t*-conformer is weakened. Furthermore, the decreasing energy of

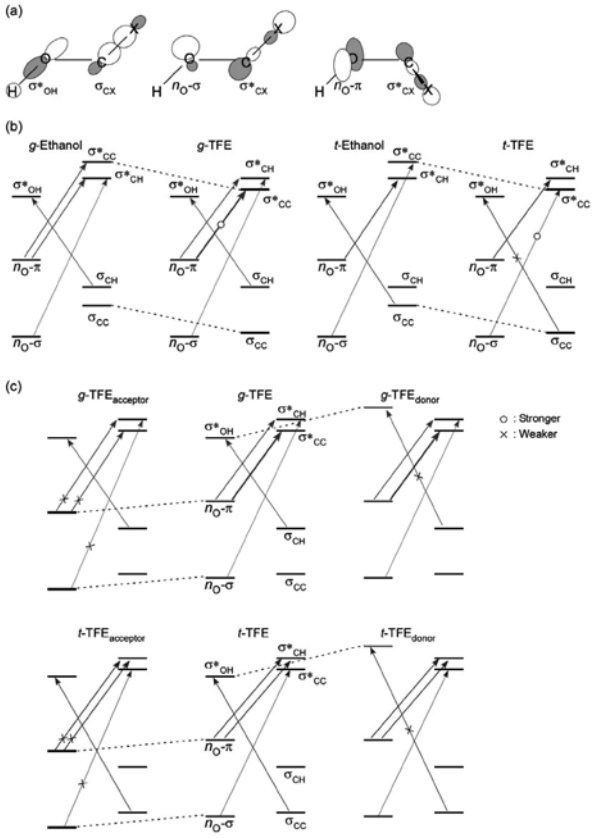

Fig. 11. (a) Schematic orbital depictions of hyperconjugation dominantly involved in the conformational preference of TFE. (b) Energy diagram of the orbitals involved in the conformational preference of gauche (left side) and trans (right side) conformers for Ethanol and TFE. The arrows mean hyperconjugative donor-acceptor electron transfer. The thick lines in TFE correspond to the CC antibonding and bonding orbitals reduced by the CF_3 substitution. The circle and cross on the arrows mean the stronger and weaker interactions in TFE than those in ethanol, respectively. For emphasis on the interaction change, the stronger interaction between n_O-π and σ*$_{CC}$ is schematically expressed as the thick arrow. (c) Energy diagram of the orbitals involved in the conformational preference of TFE in monomer (middle), H-bond acceptor (left) and H-bond donor cases (right). The thick lines correspond to the mainly altered orbitals in terms of the H-bond formation. The circle and cross on the arrows mean the enhancement and reduction of the interaction by the H-bond formation, respectively. The thick arrows in middle and right sides indicate the dominant interaction between n_O-π and σ*$_{CC}$ orbitals.

σ*$_{CC}$ leads to the stronger interaction of n_O-π → σ*$_{CC}$ (at the gauche position to the OH bond, g) for *g*-TFE, as indicated by the thick arrow. These two facts predict that *t*-TFE becomes unstable.

From the viewpoint of hyperconjugation of σ$_{CC}$(t) → σ*$_{OH}$ in *t*-TFE, one easily predicts that the it becomes weaker when TFE acts as an H-bond donor. As shown in the right side of Fig. 11(c), that is because the orbital energy of σ*$_{OH}$ ascends due to the intermolecular charge transfer from n_O-π/-σ in an H-bond acceptor molecule to σ*$_{OH}$ in TFE, which is well-known as an important term in examining the H-bond strength[38]. On the other hand, the interaction of n_O-π → σ*$_{CC}$(g) is retained to be dominantly strong, as shown by the thick arrow. In contrast to the H-bond donor, the left of Fig. 11(c) explains that n_O-π and n_O-σ in the acceptor case become lower by the repulsion with σ*$_{OH}$ in an H-bond donor molecule. Then, it leads to the weakened interaction of n_O-π → σ*$_{CC}$(g) and to the less stable *g*-TFE than monomer. In addition to the less stability of *g*-conformer, no change in the energy gap between σ*$_{OH}$ and σ$_{CC}$, which is responsible for the dominant interaction of the *t*-conformer stability, provides the relatively favorable *t*-conformation, compared to bare TFE and H-bond donor case. Although there are many complicated effects which we should take into account more distinctly, for example, the dependence of the energy change and the rehybridization of molecular orbitals on the conformation or the H-bond strength, the simple explanation focusing on the hyperconjugation of the restricted orbitals gives us a comprehensible picture and seems to be sufficiently valid.

Solvation order of mixed cluster

Another intriguing issue is the solvation order of the mixed TFE-W clusters. In both the cases of 2FP-TFE_1W_n (n = 1, 2), the most stable isomers are calculated to be C-wgF and D-wwg, respectively, corresponding to the chain structure in the order of 2FP(-W)$_n$-TFE (n = 1, 2), where *g*-TFE lies at the terminal position of the solvent network. We should elucidate a question why TFE prefers to locate at the terminal position in the mixed clusters.

Firstly, we compare each binding energy among 2FP and solvents, such as 2FP-W_1, 2FP-TFE_1 and TFE_1-W_1. As indicated by the small difference in the

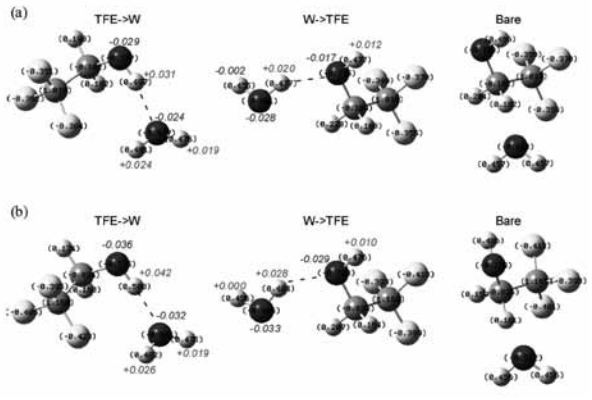

Fig. 12. Atomic charges of bare g-TFE and water, and their H-bonded clusters estimated by the natural bond orbital analysis at (a) B3LYP/6-311++G** and (b) MP2/6-311++G** levels. The H-bonded clusters are classified into TFE->W and W->TFE, where the OH group of TFE acts as H-bond donor and acceptor, respectively. The values inserted in the figure mean the variation in electron density upon the cluster formation.

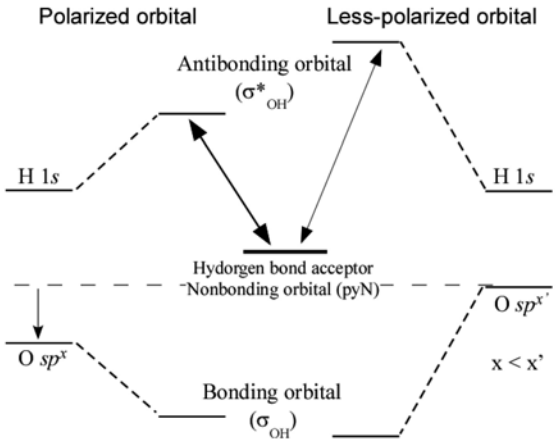

Fig. 13. A schematic energy diagram for charge transfer interaction involved in hydrogen-bond in the case of the polarized and less-polarized bonding and antibonding orbitals composed of hybrid orbitals in the oxygen atom (O sp^x) and *1s* orbital of the hydrogen atom (H *1s*). The energies of OH bonding (σ_{OH}) and antibonding (σ^*_{OH}) orbitals are expressed by repelling between O sp^x and H 1*s*. This energy gap is large in the polarized orbital rather than the less-polarized orbital, resulting in the decreasing energy of the σ^*_{OH}. Consequently, smaller energy gap between σ^*_{OH} and acceptor orbital, i.e. nonbonding orbital of pyridyl nitrogen atom (pyN) leads to the stronger hydrogen bond toward 2FP, as expressed by the thick double-headed arrow.

relative energies between C-wg and C-wgF, the additional weak interaction including C(6)-H is so small that the H-bonds between OH···pyN and between TFE and water are main factors determining the cluster stability. Then, the basicity (or proton affinity, PA) and acidity (Pk_a) of TFE and water are good indicators to estimate the H-bond strength as H-bond acceptor and donor, respectively. Especially, as shown by Leutwyler et al.[66], the measured gas-phase PA is strongly associated with the H-bond strength in H-bonded clusters. The fact that PA of water and TFE are 691 and 700.2 kJ/mol[67], respectively, expects the stronger H-bond acceptor of TFE. Pk_a of TFE in dimethyl sulfoxide solution, 23.5[68] is smaller than that of water, 31.4[69], which provides the tendency that TFE forms a stronger H-bond. For instance, comparing the calculated binding energies of 2FP-W_1 and -TFE_1, the former exhibit the 1.6 times larger value, 6.19 kcal/mol, than the latter, 3.90 kcal/mol. Thus, it is predicted that TFE can form stronger H-bonds as both the donor and acceptor. If it is so, the solvation order in which TFE is inserted between 2FP and water seems to be of advantage, which contradicts the overall cluster stability. Thus, it is inadequate to compare each H-bond strength.

Secondly, it is necessary to consider the induced polarization (or molecular orbital change) of each OH group in the chain structure, which is well-known as cooperative effect[38,70]. Based on the natural population estimated by the natural bond orbital (NBO) analysis, we discuss the charge variation of the OH groups by the H-bond formation of C-wg and C-gw for 2FP-TFE_1W_1. Figure 12 shows the atomic charge of the bare *g*-TFE and water, and their H-bonded clusters, which are obtained at the B3LYP and MP2 with 6-311++G** basis set. Here, it is worthwhile mentioning that the atomic charge of NBO analysis is sensitively dependent on the calculation levels and basis sets. Then, this article demonstrates two different calculation results. However, both exhibit almost same trend, so that we consider our following discussion based on this NBO analysis to be reasonable. The H-bonded clusters are classified into

two types; one is TFE->W meaning that TFE donates a hydrogen atom to the oxygen atom in water, the other is vice versa, W->TFE. The values inserted in the figure denote the increase and decrease of the electron density from those of bare ones. The atomic charges on the oxygen and hydrogen atoms of water moiety in the case of TFE->W are more largely perturbed than those of TFE moiety in W->TFE.

As well described in Fig. 13, this large polarization has been interpreted to induce the energy reduction of antibonding OH orbital (σ^*_{OH}) due to the larger energy gap between the 1*s* orbital on hydrogen atom and the hybrid one (O sp^x) on oxygen atom composed of the larger contribution of 2*s* one. In other words, the more polarized σ_{OH} and σ^*_{OH} consist of O sp^x (x < x'), which lowers the energy of σ^*_{OH}. Since the energy gap between σ^*_{OH} and the nonbonding orbital of pyN plays an important role in determining the H-bond strength, since the second-order perturbative energy $E_{ij^*}^{(2)}$ caused by the charge transfer from the H-bond acceptor orbital *i* to the antibonding orbital *j** of H-bond donor is expressed in NBO as eq. (1) [71].

$$E_{ij^*}^{(2)} = -n_i^{(0)} \frac{\left\langle \phi_i^{(0)} \middle| \hat{F}_{KS} \middle| \phi_{j^*}^{(0)} \right\rangle^2}{\varepsilon_{j^*}^{(0)} - \varepsilon_i^{(0)}}, \qquad (1)$$

where $\phi_i^{(0)}$ and $\phi_{j^*}^{(0)}$ are the zeroth-order wave function of the H-bond acceptor orbital and the antibonding orbital, respectively, ε_i and ε_{j^*} are the zeroth-order energies of each orbital, $n_i^{(0)}$ is the occupancy in the orbital *i*, and $\hat{F}_{KS}$ is the Kohn-Sham form of the one-electron effective Hamiltonian. Consequently, the decreasing energy of σ^*_{OH} implies that the free OH group of water in TFE->W is able to form the stronger H-bond with 2FP, leading to more stable C-wgF. Moreover, it is predicted that, even in the case of increasing the number of water solvents, the induced polarization by the terminal TFE preferably stabilizes the cluster. This prediction agrees well with the obtained result that D-wwg is the most stable isomer.

In conclusion, we regard cooperative effect as dominant factor determining the solvation order in TFE-W mixture rather than H-bond acceptor or donor abilities of TFE and water. Furthermore, we consider the solvation order to be very important to elucidate the preference of the terminal TFE in the H-bond network. That is because these results in the gas phase may be available to understand the H-bond network structure around peptides or proteins in TFE-W mixed solution, furthermore may support for us to elucidate the mechanism of alcohol denaturation or the stabilized secondary structure by alcohol-based co-solvents.

Acknowledgment

This work is supported by the Grant-in-aids for Young Scientist (A) (Grant no. 22750020) by from the Ministry of Education, Culture, Sports, Science, and Technology (MEXT).

Reference

[1] H. Sticht, D. Willbold and P. Rösch, *J. Biomol. Struct. Dyn.* **12**, 19 (1994).
[2] R. M. Ionescu and C. R. Matthews, *Nat. Struct. Biol.* **6**, 304 (1999).
[3] M. J. Howard and C. M. Smales, *J. Biol. Chem.* **280**, 22582 (2005).
[4] A. Jasanoff and A. R. Fersht, *Biochemistry* **33**, 2129 (1994).
[5] M. Q. Buck, *Rev. Biophys.* **31**, 297 (1998).
[6] J. F. Povey, C. M. Smales, S. J. Hassard and M. J. Howard, *J. Struct. Biol.* **157**, 329 (2007).
[7] T. V. Naumenkova, O. V. Levtsova, I. N. Nikolaev and K. V. Shaitan, *Biophysics* **55**, 32 (2010).
[8] M. Fioroni, M. D. Diaz, K. Burger and S. Berger, *J. Am. Chem. Soc.* **124**, 7737 (2002).
[9] V. L. Anderson, T. F. Ramlall, C. C. Rospigliosi, W. W. Webb and D. Eliezer, *Proc. Natl. Acad. Sci. USA* **107**, 18850 (2010).
[10] D.-P. Hong, M. Hoshino, R. Kuboi and Y. Goto, *J. Am. Chem. Soc.* **121**, 8427 (1999).
[11] M. Buck, S. E. Radford and C. M. Dobson, *Biochemistry* **32**, 669 (1993).
[12] Y. Yang, S. Barker, M. J. Chen and K. H. Mayo, *J. Bio. Chem.* **268**, 9223 (1993).
[13] D. Roccatano, G. Colombo, M. Floroni and A. E. Mark, *Proc. Natl. Acad. Sci. USA* **99**, 12179 (2002).
[14] D. H. Levy, *Ann. Rev. Phys. Chem.* **31**, 197 (1980).
[15] H. Abe, N. Mikami and M. Ito, *Chem. Phys. Lett.* **215**, 1768 (1982).
[16] a) S. Tanabe, T. Ebata, M. Fujii and N. Mikami, *Chem. Phys. Lett.* **215**, 347 (1993). b) T. Watanabe, T. Ebata, S. Tanabe, and N. Mikami,

J. Chem. Phys. **105**, 408 (1996).

[17] a) G. V. Hartland, B. F. Henson, V. A. Venturo and P. M. Felker, *J. Phys. Chem.* **96**, 1164 (1992).

[18] A. K. Kim, S. C. Hsu, S. Li and E. R. Bernstein, *J. Chem. Phys.* **95**, 3290 (1991).

[19] M. Schültz, T. Bürgi and S. Leutwyler, *J. Chem. Phys.* **98**, 3763 (1993).

[20] A. G. Taylor, T. Bürgi and S. Leutwyler, *Jet spectra of aromatic molecules in hydrogen bonded microsolvent clusters in Jet spectroscopy and molecular dynamics,* eds. J. M. Hollas and D. Phillips (Chapman & Hall, Blackie Academic, London, 1994), pp 151-180.

[21] a) R. N. Pribble and T. S. Zwier, *Science* **265**, 75 (1994). b) C. J. Gruenloh, J. R. Carney, C. A. Arrington, T. S. Zwier, S. Y. Fredericks and K. D. Jordan, *Science* **276**, 1678 (1997).

[22] a) R. Wu, P. Nachtigall and B. Brutschy, *Phys. Chem. Chem. Phys.* **6**, 515 (2004).

[23] T. Ebata, *Bull. Chem. Soc. Jpn.* **82**, 127 (2009).

[24] Y. Yamada, Y. Katsumoto and T. Ebata, *Phys. Chem. Phys. Chem.* **9**, 1170 (2007).

[25] R. J. Lipert and S. D. Colson, *J. Phys. Chem.* **93**, 135 (1989).

[26] A. H. Zewail, *Faraday discuss. Chem. Soc.* **75**, 315 (1983).

[27] H. Lippert, V. Stert, L. Hesse, C. P. Schultz, W. Radloff and I. V. Hertel, *Eur. Phys. J. D* **20**, 445 (2002).

[28] G. A. Pino, C. Dedonder-Lardeux, G. Grégoire, C. Jouvet, S. Martrenchard and D. Solgadi, *J. Chem. Phys.* **111**, 10747 (1999).

[29] S.-I. Ishiuchi, M. Sakai, K. Daigoku, K. Hashimoto and M. Fujii, *J. Chem. Phys.* **127**, 234304 (2007).

[30] G. A. Pino, A. N. Oldani, E. Marceca, M. Fujii, S.-I. Ishiuchi, M. Miyazaki, M. Broquier, C. Dedonder, and C. Jouvet, *J. Chem. Phys.* **133**, 124313 (2010).

[31] C. Tanner, C. Manca and S. Leutwyler, *Science* **302**, 1736 (2003).

[32] K. Sakota, N Komure. W. Ishikawa and H. Sekiya, *J. Chem. Phys.* **130**, 224307 (2009).

[33] J. Marco and J. M. Orza, *J. Mol. Struct.* **267**, 33 (1992).

[34] J. Marco, J. M. Orza and J.-L. M. Abboud, *Vibr. Spectrosc.* **6**, 267 (1994).

[35] T. Scharge, T. Häber and M. A. Suhm, *Phys. Chem. Chem. Phys.* **8**, 4664 (2006).

[36] T. Scharge, C. Cézard, P. Zielke, A. SchültzC. Emmeluth and M. A. Suhm, *Phys. Chem. Chem. Phys.* **9**, 4472 (2007).

[37] V. Venkatesan, A. Fujii, T. Ebata and N. Mikami, *J. Phys. Chem. A* **109**, 915 (2005).

[38] G. A. Jeffrey, *An Introduction to Hydrogen bonding* (Oxford University Press, New York, 1997).

[39] a) J. P. Perchard and M. L. Josien, *J. Chem. Phys.* **65**, 1834 (1968). b) J. P. Perchard, and M. L. Josien, *J. Chem. Phys.* **65**, 1856 (1968).

[40] B. J. van der Veken and P. Coppens, *J. Mol. Struct.* **142**, 359 (1986).

[41] J. R. Durig and C. W. Hawley, *J. Phys. Chem.* **75**, 3993 (1971).

[42] A. J. Barnes and H. E. Hallam, *Trans. Faraday Soc.* **66**, 1932 (1970).

[43] V. F. Kalansinsky and H. V. Anjaria, *J. Phys. Chem.* **84**, 1940 (1980).

[44] M. Perttila, *Spectrochim. Acta Part A* **35**, 585 (1987).

[45] J. R. Durig and R. A. Larsen, *J. Mol. Struct.* **238**, 195 (1989).

[46] M. L. Senent, A. Perez-Ortega, A. Arroyo and R. Domínguez-Gómez, *Chem. Phys.* **266**, 19 (2001).

[47] L.-H. Xu, G. T. Fraser, F. J. Lovas, R. D. Suenram, C. W. Gillies, H. E. Warner and J. Z. Gillies, *J. Chem. Phys.* **103**, 9541 (1995).

[48] I. Bakó, T. Radnai, M. Claire and B. Funel, *J. Chem. Phys.* **121**, 12472 (2004).

[49] P. J. Krueger and H. D. Mettee, *Can. J. Chem.* **560**, 295 (2001).

[50] M. L. Senent, A. Niño, C. Muñoz-Caro, Y. G. Smeyers, R. Domínguez-Gómez and J. M. Orza, *J. Phys. Chem. A* **106**, 10673 (2002).

[51] Y. Nibu, C. Okabe, T. Ohsaki and H. Shimada, *J. Phys. Chem. A* **110**, 6047 (2006).

[52] Y. Nibu, R. Marui and H. Shimada, *J. Phys. Chem. A* **110**, 9627 (2006).

[53] Y. Nibu, R. Marui and H. Shimada, *Chem. Phys. Lett.* **442**, 7 (2007).

[54] M. J. Frisch, G. W. Trucks, H. B. Schlegel, et al., *Gaussian 03, revision E.01,* Gaussian, Inc., Pittsburgh, PA, 2004.

[55] K. N. Wong and S. D. Colson, *J. Mol. Spectrosc.* **104**, 129 (1984).

[56] S. Abbate, S. L. Wunder and G. Zerbi, *J. Phys. Chem.* **88**, 593 (1984).
[57] F. Perakis, S. Widmer and P. Hamm, *J. Chem. Phys.* **134**, 204505 (1997).
[58] Y.-A. Yan, M. Petković, G. M. Krishnan and O. Kühn, *J. Mol. Struct.* **972**, 68 (2010).
[59] H. L. Fang and R. L. Swofford, *Chem. Phys. Lett.* **105**, 5 (1984).
[60] S. Wolfe, *Acc. Chem. Res.* **5**, 102 (1972).
[61] T. K. Brunck and Weinhold, *J. Am. Chem. Soc.* **101**, 1700 (1979).
[62] P. Dionne and M. St-Jacques, *J. Am. Chem. Soc.* **109**, 2616 (1987).
[63] P. R. Rablen, R. W. Hoffmann, D. A. Hrovat and W. T. Borden, *J. Chem. Soc., Perkin. Trans.* **2**, 1719 (1999).
[64] V. Prophristic and L. Goodman, *Nature* **411**, 565 (2001).
[65] L. Goodman, H. Gu and V. Pophristic, *J. Phys. Chem. A* **109**, 1223 (2005).
[66] C. Wickleder, D. Henseler and S. Leutwyler, *J. Chem. Phys.* **116**, 1850 (2002).
[67] E. P. L. Hunter and S. G. Lias, *J. Phys. Chem. Ref. Data* **27**, 413 (1998).
[68] F. G. Bordwell, *Acc. Chem. Res.* **21**, 456 (1988).
[69] W. N. Olmstead, Z. Margolin and F. G. Bordwell, *J. Org. Chem.* **45**, 3295 (1980).
[70] K. Sakota, Y. Kageura and H. Sekiya, *J. Chem. Phys.* **129**, 054303 (2008).
[71] F. Weinhold and C. Landis, *Valency and Bonding* (Cambridge University Press, Cambridge, 2005).